PROCEEDINGS, 49th Workshop on Geothermal Reservoir Engineering
Stanford University, Stanford, California, February 12-14, 2024
SGP-TR-227

Characterization of Thermal Ground at the Roosevelt Hot Springs Hydrothermal System, Utah

Aileen Zebrowski and Brian J. McPherson

Civil & Environmental Engineering, 110 Central Campus Drive, Suite 2000, University of Utah, Salt Lake City, UT 84112

b.j.mcpherson@utah.edu

Keywords: geothermal, hydrothermal, reservoir, fault, heat flow, flash steam

ABSTRACT

The Blundell geothermal power plant, located near Milford, Utah, is driven by the Roosevelt Hot Springs hydrothermal system. The plant consists of two units: a single-flash steam plant that has been in operation since 1984, and a binary plant commissioned in 2007. Blundell produces more groundwater from the reservoir than it reinjects, primarily due to evaporative losses from the plant's cooling towers, resulting in a net fluid loss of about 3 billion lbs/yr. Consequently, a net pressure decline in the reservoir of approximately 40 bar over the course of Blundell's operation is observed. We hypothesize that this pressure drop is causing drawdown of the water table, an increase in steam within the vadose zone, and subsequently forming an area of steam-heated thermal ground. Elevated soil temperatures are observed approximately 1 km north of the power plant, where the Opal Mound and Mag Lee Faults intersect. Across an area of about 1 square km, shallow soil temperatures (8 inches deep) exceed the local background levels, with the highest measurements reaching the local atmospheric boiling point (approximately 94°C). The thermal ground is associated with an extensive network of steam vents, along with dead vegetation observed in areas with the hottest soil temperatures. The extent of the thermal ground is actively increasing, and this paper attempts to delineate the thermal expansion that has occurred from 2012 to the present.

The purpose of this study is to test the hypothesis that groundwater production at the Blundell power plant is the cause of the thermal ground formation and its subsequent expansion over time. Previous studies have surveyed surface temperatures (T_{surf}) and CO_2 fluxes (QCO_2) across the area of interest. To quantify the temporal variation of these parameters, we conducted additional T_{surf} and QCO_2 field surveys across multiple seasons in 2022-2024. These recent data, normalized to background conditions, were compared to corresponding normalized datasets from 2012 (T_{surf}) and 2017-2018 (QCO_2). The comparison reveals a decade-long increase and expansion in surface soil temperatures concentrated around three hotspots within the thermal field.

1. INTRODUCTION

Roosevelt Hot Springs (RHS), a hydrothermal system near Milford in southwest Utah, is situated along the western foothills of the Mineral Mountains within the Basin and Range geological province, a region of tectonic extension faulting (Knudsen et el., 2019. The subsurface reservoir has peak temperatures between 250-270°C, and supplies heated fluid to the Blundell geothermal power plant, commissioned in 1984 (Allis et al., 2015). The original power plant, which is still in use today, is a flash-steam plant that currently produces 23 MW of net electricity to the grid. In 2007, a binary cycle power plant was integrated into Blundell's operations and supplies an additional 10 net MWe. 85% of the produced geothermal fluid is reinjected, while the rest (approximately 3 billion lbs/yr) is lost due to evaporation at the cooling towers, resulting in a net pressure decline in the reservoir. The most significant decline in pressure (>30 bar) occurred during the first six years of operations, during which time thermal ground and fumarolic activity was first observed in response. An increase in vertical extent of subsurface steam above the reservoir has also been observed (Allis and Larsen, 2012).

The reservoir is nestled at the intersection of two sub-vertical faults, the north-south trending Opal Mound Fault (OMF) and the east-west trending Mag Lee Fault (MLF) (Figure 1). Both faults terminate at this intersection, creating a series of fault splays to the north. The reservoir is recharged by deep circulation of meteoric water from the Mineral Mountains, which is heated by a magmatic intrusion at depth (Faulder, 1991), and then upwells along the hydraulic boundary formed by the OMF. The fluid exits the system via a shallow outflow plume to the north at a rate of approximately 60 kg/s, and to a lesser extent via an outflow plume to the south (Allis et al., 2019).

A spring previously existed to the north of the reservoir, above the outflow plume. Roosevelt Hot Spring, the namesake for the hydrothermal system, flowed at a rate of approximating 1 kg/s (2% of the entire system flow) at near boiling temperatures. The resultant heat output through the surface through this liquid spring was approximately 300 kW. The rest of the fluid exited the system via the subsurface. A resort once existed at the hot spring in the late 1800's to early 1900's (Allis et al., 2019), but the spring ceased to produce surface water sometime between 1957 and 1970 (Nielson, 1986). Following the commencement of power production activities, a subsurface steam zone formed over the liquid reservoir and the former hot spring location became the site of steaming ground (Allis and Larsen, 2012). Nearly a square kilometer of thermal and steaming ground now exists north of the reservoir, with heat loss now estimated to be 10 MW through the surface (Allis et al., 2019).

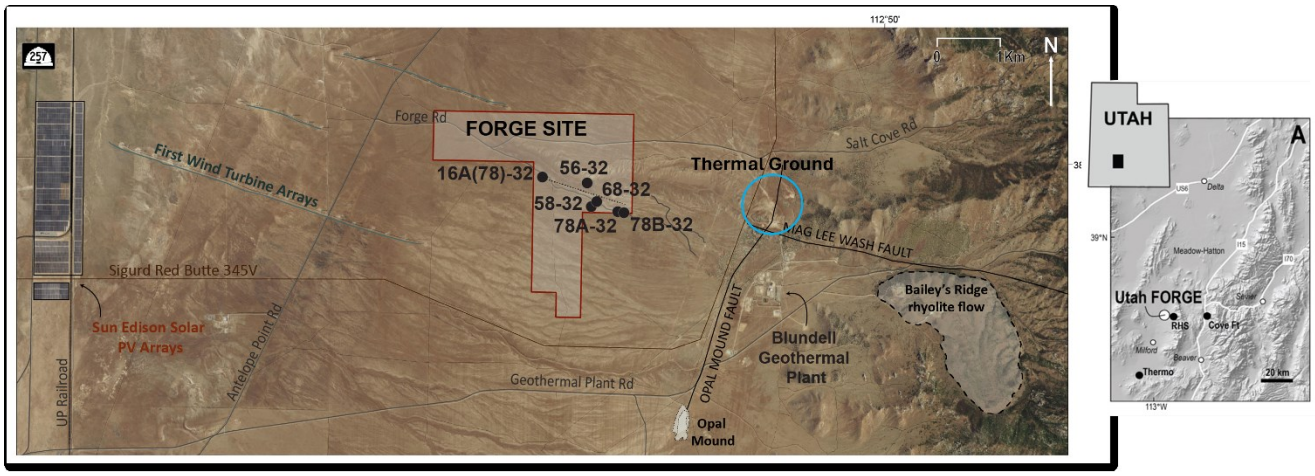

Figure 1. Site location map of the thermal ground (circled) and surrounding features, including the Opal Mound and Mag Lee Faults. This map also identifies elements of the renewable energy corridor, including the Blundell geothermal power plant, and the Utah FORGE geothermal research site (and associated wells), and wind and solar arrays.

Previous characterization studies of the thermal ground include a 2012 soil temperature survey by Allis et al., (2019), and a 2017/2018 CO_2 soil flux survey conducted as part of the Utah FORGE site characterization (Rahilly et al., 2019; utahforge.com). The extent and degree of the thermal anomaly were quantified based on the soil temperatures measured at 8 inches depth, and a contour map was generated to visualize the results. While additional thermal anomalies were identified along the OMF during the 2012 temperature survey, the most prominent anomaly is the steaming ground located over the fault splays to the north, and this area is the focus of the current study. The contour map displayed in Figure 2 is an adjusted version of the plot generated by Allis et al. (2019) and is constructed from the same dataset. Presented in this paper are the results of repeated temperature surveys over multiple seasons to quantify the seasonal and decadal scale changes in the thermal anomaly. CO_2 soil flux measurements were also taken across transects of the thermal ground as part of this characterization study, however, they are not analyzed here.

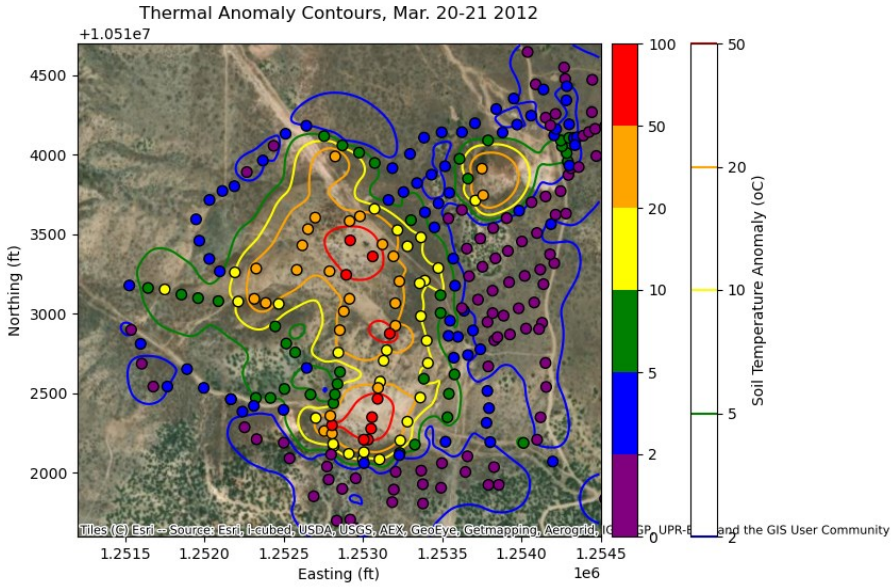

Figure 2: Data from the original Allis et al., (2019) temperature survey of the Roosevelt Hot Springs, performed in March of 2012. The interpretation of the thermal anomaly contours (temperature difference above background) was generated using a kriging procedure, as presented in the paper below, and may not precisely align with the original contour map.

2. FIELD METHODS

Soil temperature measurements were taken at 8 inches depth across the thermal ground during six field survey periods: October 2022 (two surveys), January 2023, March 2023, October 2023, and January 2024. During the first October 2022 survey, data was collected along a 75-m grid encompassing the same region surveyed by Allis et al. (2019). Three hot spots were identified exceeding 90°C in this initial survey, leading to a subsequent October 2022 survey where data was collected along 25-m grids over these three hot spots to capture areas exhibiting the most significant temperature changes. In January 2023, the 75-m grid was surveyed again, along with two intersecting 25-

m transects across the field, which provided finer resolution through two of the hot spots. The March 2023 survey was limited to the same two major 25-m transects, and select minor transects across the hot spots. This survey was limited because it was taken concurrently with a drone survey performed by the Utah Geological Survey (UGS) that measured ground surface temperature. To improve the drone survey results, and to improve the correlation between surface and subsurface data, the soil temperature readings were taken in the early morning, mostly before sunrise, to limit solar thermal effects on the ground surface. The October 2023 and January 2024 surveys repeated measurements across the 75-m grid (with some low temperature peripheral points eliminated), as well as all 25-m transects (major and minor) measured in March 2023.

To quantify the degree and extent of the thermal anomaly, the temperatures measured at the thermal ground must be compared to background soil temperatures. Background soil temperature readings were taken two or three times each day during a given survey trip: at the beginning of the field day, and the end of the field day, and midday when warranted. Background readings were taken at three locations, labeled as B-1, B-2, and B-3, and each spot is located at a distance of 0.5 km or greater from the thermal field. During the 2012 survey, a background base station was also established for this purpose, approximately 4 km south of the current background locations. However, measurements taken near B-1, B-2, and B-3 during the 2012 survey varied by less than 1°C from the base station readings.

CO_2 soil flux surveys were also taken in January, March, and October of 2023, and January 2024. These measurements were taken using a LI-8100 Automated Soil CO_2 Flux System. Seventeen soil collars are placed at 75-m intervals along a north-south and east-west transect, as well as three background collars and a bonus high flux collar. These collars remain on-site between surveys but are checked and secured the day prior to gathering CO_2 readings. Any loose collars are hammered back into the ground. CO_2 concentrations were measured over 60-90 second intervals in triplicate at each collar location, and soil flux was calculated based on these readings.

3. ANALYSIS METHODS

The background temperature is taken to be the average of the soil temperature measurements at the three background locations, B-1, B-2, and B-3. The thermal anomaly at each sample location is then calculated as the difference in measured temperature above this average background temperature. To account for the diurnal variability in background soil temperatures, linear interpolation is used to estimate the background temperature throughout the day between the discrete background measurements.

Two methods of interpreting the temperature data are considered. The first method is to quantify the thermal anomaly. This follows the method used by Allis et al., (2019) to represent the data, where the temperature anomaly is the difference between the raw temperature measurement and the background temperature. The second interpretation method is to normalize the soil temperature of each data point on a relative scale between the background temperature and the local boiling point (about 94°C). The normalized soil temperature (T_{norm}) is calculated using the equation below:

$$T_{norm} = \frac{T_{raw} - T_{bkg}}{T_{BP} - T_{bkg}} \quad (1)$$

where T_{raw} is the raw soil temperature measured, T_{bkg} is the background temperature, and T_{BP} is the boiling point temperature, estimated to be 94°C based on the elevation of the field site (generally 1800-1850 m above mean sea level (asl)) and the maximum temperature measured on-site during the recent surveys.

Contour maps were generated by kriging using the python libraries skgstat and gstools. This results in an output grid of interpolated temperatures across the field site. To better visualize how this output changes between seasons and years, the interpolated temperature distributions from different field campaigns were subtracted from each other and plotted as a heat map. Another approach to interpreting the data was to plot the calculated temperatures measured along the two major transects.

4. RESULTS

4.1 Background Temperature Data

Figure 3 portrays the method for calculating the background soil temperature throughout the day by averaging the manual readings at each of the three background locations, and interpolating between them. Specifically, Figure 3 shows an example process from the January 2023 field trip. The top two plots (Figure 3A.) show the individual soil and air background temperature readings collected at locations B-1, B-2, and B-3. As a baseline, the plots also include the 4-inch soil temperature data collected at a weather station in Milford, Utah, which is located 18 km to the southwest of the field site and is 300 m lower in elevation. In the bottom two plots, Figure 3B, the average background temperatures are plotted, along with linear interpolation between these average values and the corresponding standard deviation. The minimum and maximum average background temperatures calculated in this way during each field trip is summarized in Table 1. Occasionally, an additional B-3 measurement was taken beyond those taken at B-1 and B-2. While this can help delineate the diurnal temperature trends, because of variability between the three background locations, these extra readings were not included in the linear interpolation as it skews the average background temperature value.

.

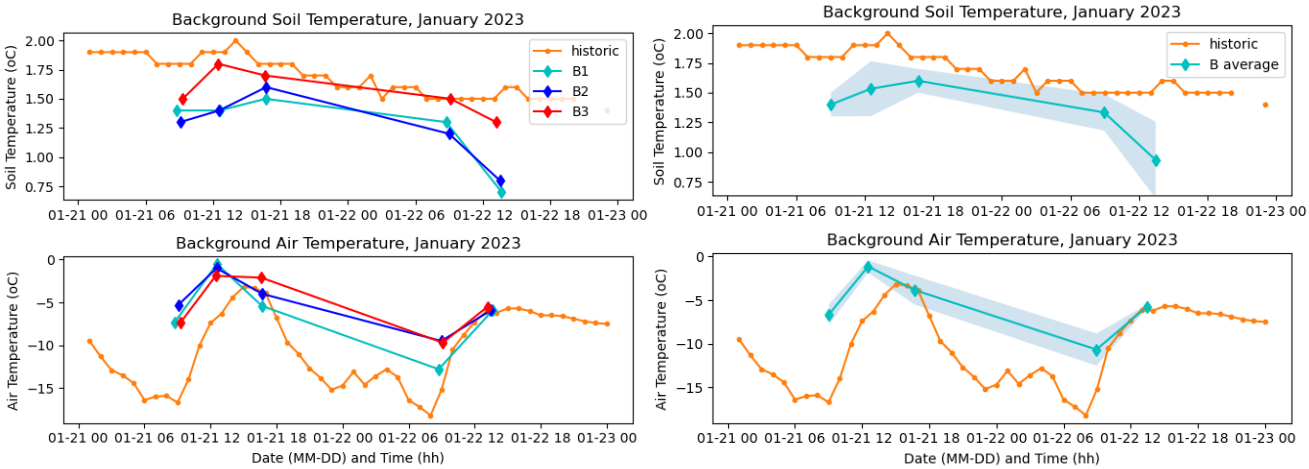

Figure 3: Background soil (top) and air (bottom) temperatures over time during the January 2023 field sampling trip to the Roosevelt Hot Springs thermal ground. The left plots show discrete manual background measurements, represented by diamonds, with each background sample location depicted by a different color (B-1 is cyan, B-2 is blue, and B-3 is red). Measurements from each sample location are connected by a line. The right plots show the averaged background temperatures (soil and air) across the three sample locations (B-1, B-2, and B-3) for each background sampling interval (always within a 40-minute window or less). Also depicted is the linear interpolation between each background temperature value, and a fill line depicting the standard deviation. All plots include hourly readings from the Milford weather station (with soil temperatures taken at 4-in depth). These weather station data are represented by orange circles with linear interpolation between sequential hourly readings.

Table 1: Minimum and maximum background temperatures used to process data from each field trip, based on the average of the measurements taken at B-1, B-2, and B-3. Includes 2012 base station data.

Field Trip Dates	Background Soil Temperature (°C)	
	Min	Max
March 20-21, 2012	3	6
October 12-14, 2022	17.8	21.4
October 29-30, 2022	6.4	8.7
January 21-22, 2023	0.9	1.6
March 24-25, 2023	1.7	4.6
October 21-22, 2023	16.7	19.3
January 19-20, 2024	2.5	4.0

4.2 Temporal Trends in Surface Temperature Distribution

The contour plots shown in Figure 4 represent the thermal anomaly distribution interpolated across the field using a kriging method. The thermal anomaly was chosen to be represented here to match the interpretation method used by Allis et al., (2019). A plot was made for each of the recent six temperature surveys, as well as the re-processed data from 2012. The kriging procedure is more effective the greater the sampling density as it can interpolate between known points. Consequently, this method does not accurately interpolate the temperature conditions beyond the extent of the sampled thermal field. The contour plots currently indicate that thermal anomalies exist as the background condition, which, by definition, is false. Therefore, the exact extents of the thermal field cannot be accurately delineated using this method with the current sample set, and any background coloring should be neglected.

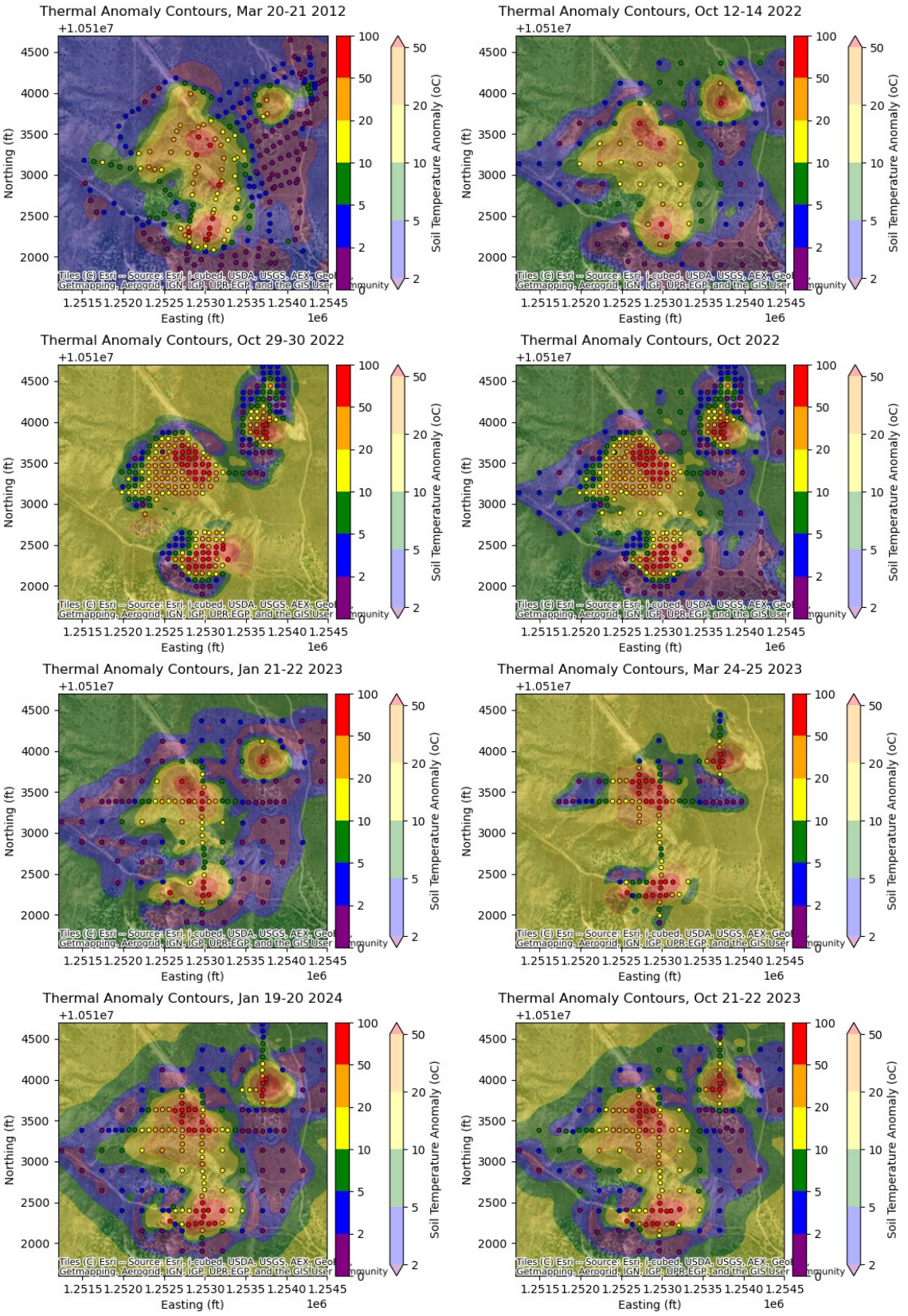

Figure 4: The interpolated thermal anomaly contours generated by kriging, overlaying a satellite image from ESRI World Imagery. Each figure is from a different survey field trip, and they are presented in chronological order. Each dataset is processed under the same kriging input parameters, including March 2012 data. A bonus plot includes the combined results of the two October 2022 survey trips.

4.3 Trends in Cross-Section

The temperature trends can also be monitored along transects over time. The surface temperature data along two transects in particular were taken during every field trip, often at 25-m intervals. These two transects, referred to here as the "major transects", are perpendicular to each other, with one trending north-south and the other east-west. The major transects each cross one or two of the hotspots through the middle of the thermal field, and the transects intersect at the sample point 41. Figure 5 depicts the temperature distribution along these two transects during each of the recent six field surveys.

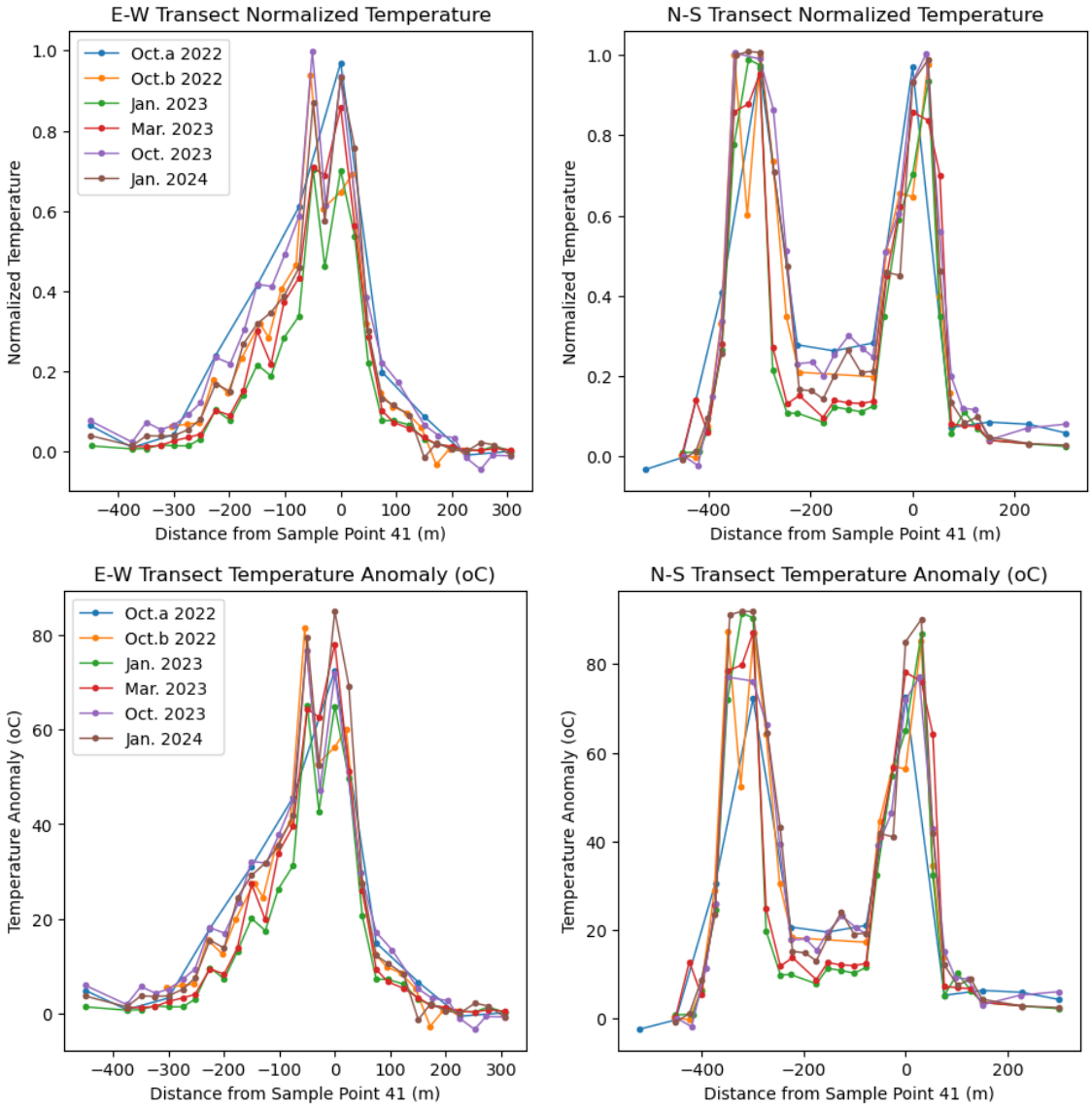

Figure 5: Soil thermal anomaly data along the major north-south and east-west transects through the thermal field. The x-axis represents the distance of the sample location to sample point 41, the point at which the two transects intersect. Positive distance represents points north of 41 in the N-S transect (right), or points east of 41 (left). Each circle represents a discrete sample location and corresponding temperature. Each color represents a separate field trip, with Oct. a 2022 being the earlier of the two trips, and Oct. b being the later. The upper figures are the normalized temperature, while the lower figures represent the thermal anomaly above background levels. Each color represents a separate field trip.

5. DISCUSSION

5.1 Seasonal Comparisons

When evaluating the transect plot (Figure 5), a correlation can be found between the relative temperature measurements for a given field trip and the corresponding background temperatures recorded. This trend is most apparent at lower temperatures and where the temperature changes are more gradual. This occurs east of point 41, and in the center of the N-S transect. January 2023 data is generally the coldest, followed by March 2023, and the three October datasets are also generally segregated based on their corresponding background temperatures, per Table 1. The exception comes from the latest field survey, January 2024, where the temperature trend for this survey

exceeds January and March 2023, and in fact is closer to the Oct. b. 2022 data trend, despite having a background temperature 4-5°C cooler. The reason for this anomaly may have to do with climactic variation, since the 2023/2024 winter was far milder and drier than the previous year. It may also be in part due to a trend of warming in the field.

These transect plots are also informative on the effectiveness of the two temperature correction procedures. The thermal anomaly appears to be a more appropriate comparison tool when the soil temperatures are relatively low, as the seasonal data exhibits less variability below around 50-60°C (0.5 normalized). As the temperatures approach the upper threshold, the boiling point, the normalized temperatures becomes more useful. The thermal anomaly trends swap at higher temperatures, with the lower background temperature trips experiencing greater thermal anomalies. This is expected since the maximum possible thermal anomaly is greater when the initial conditions are colder. Meanwhile, normalized temperatures loosely follow the same trend at all temperatures.

Temperature corrections were an attempt to directly compare datasets across seasons. While these methods are sufficient to correct for diurnal variation in the background readings, it is clear from analyzing the transect results that these methods are not adequate in accounting for seasonal and climactic variations. Alternative methods will be necessary to correct for additional outside influences to the thermal field. The goal is to isolate the influence of the subsurface on the field extents and temperature distribution.

5.2 Contrasts in Annual Values

The transect results demonstrate that cross-seasonal data is not directly comparable following the current approach. Therefore, to get a more accurate signal of the long-term temperature trends over time, surveys that were performed during the same season across different years can be compared to see if annual scale changes can be detected. Field surveys from October and January spanning two different years are therefore used for this analysis. To visually compare the differences in three-dimensions, the kriging results for an earlier year are subtracted from the results from a later year to generate a single figure which highlights the differences between the two.

To minimize sampling bias, only sample locations measured during both years are included in the comparison process. For example, the October 2023 sample set consists of measurements along the 75-m grid and select 25-m transects. To achieve a matching dataset with the previous year, the survey data from the two October 2022 surveys were combined and then filtered to only include data points that were also sampled in 2023. Filtering was also performed on the January datasets to exclude minor transects sampled in 2024 and not 2023.

The annual recorded differences are shown in Figure 6, with the blue shades indicating that the temperature decreased over the year, and red shades indicating that the temperature increased over the year.

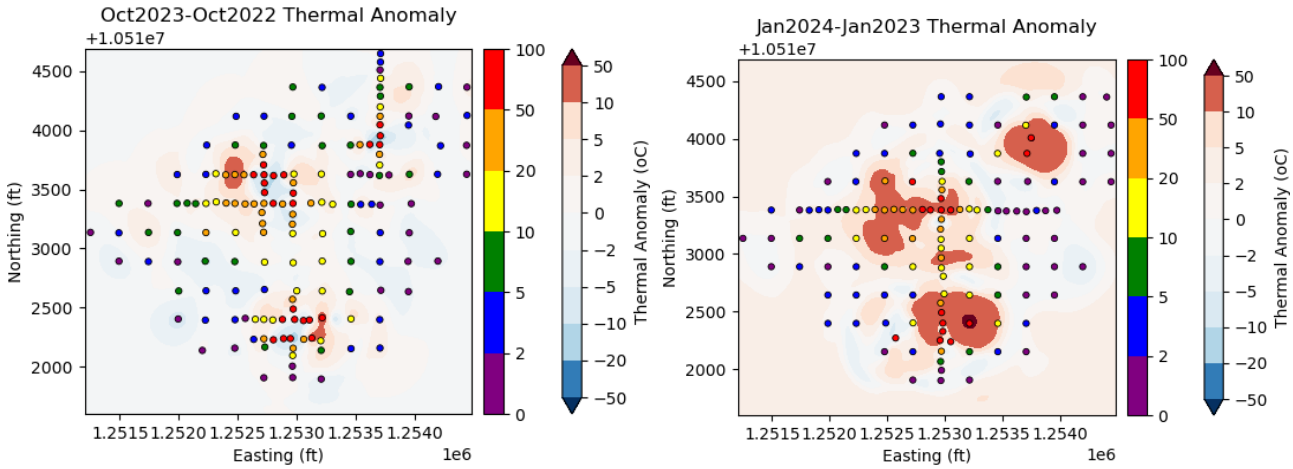

Figure 6: Heat map depicting the difference between the thermal anomaly interpolated across the thermal field between October 2023 and October 2022 (left) and January 2024 and January 2023 (right). Blue values indicate a decrease in temperature, while red values indicate an increase in temperature. The sample locations are represented by circles on the map, and colored based on the most recent temperature results.

The observed differences between the 2022 and 2023 October datasets are minimal across most of the field. However, a notable increase in temperature is observed around the periphery of the hotspots. This observation suggests that the hotspots are indeed growing outwards, while the temperatures across the rest of the field is fairly stagnant. A faint cold signature is also apparent in the center of the hotspots as well. While this could indicate cooling temperatures, it is more likely an artifact of using the thermal anomaly method instead of normalized temperature at the very hottest spots. As was observed in the transect data, the thermal anomaly becomes more sensitive to the background temperature than the raw temperature when it approaches boiling, and these blue patches are correlated with the highest temperature (red) points on the map.

The observed differences between the 2023 and 2024 January datasets are similar in distribution to October, but far more significant in extent. This warming signature, however, is likely to be at least in part due to the warmer, drier conditions present in January 2024 than 2023. This weather variability presents an added challenge to interpreting the data. However, between the significant temperature increases

observed, in conjunction with a similar (though muted) signature observed in the October data, it seems likely that the hotspots are indeed expanding outwards. The temperature distribution across the rest of the field on the other hand is far less definitive, but appears to be holding relatively stagnant, or potentially cooling slightly based on the broad regions of light blue across the study area in both plots.

5.3 Decadal Variability

To see if these annual observed temperature changes have been consistent over the past decade, the same approach was taken to compare the recent survey data to that of the March 2012 survey. There is not a large March 2023 dataset available to compare with the 2012 dataset, however, the data available was still processed for comparison, with results shown in Figure 7. The results suggest that parts of the major transects are getting colder, but conversely, there is an observable increase in the hot spot extents. This matches with the warming signals noted in the October and January comparisons in Figure 6. To test this observation across the entire field on a more complete dataset, a comparison between January 2023 and March 2012 was also performed. This comparison is reasonable since the January 2024 background temperatures are comparable to those from the March 2023 survey. Thus the January dataset can serve as a reasonable, if not conservative, proxy in for March data. Despite being a conservative comparison, there is still a strong signal of warming around the hot spots, matching those from the March 2023 comparison. Temperature stagnation is also still observed in most of the rest of the field, with slight cooling possible. The strongest cooling signature is located near the central N-S transect, and while cooling is possible, sampling bias may also play a role. Between the recent and 2012 datasets, sampling bias cannot be avoided since the sample locations do not align. Additionally, it is noted that the 2012 samples collected near this transect appear to follow topographic features, which could be impacting the measured temperatures.

The annual and decadal results both provide evidence that the hot spots are expanding over time. This conclusion is further supported by satellite images of the field, which show an outward growth of surface discoloration over time, particularly the northeast hotspot. A comparison of satellite images is presented in Figure 8.

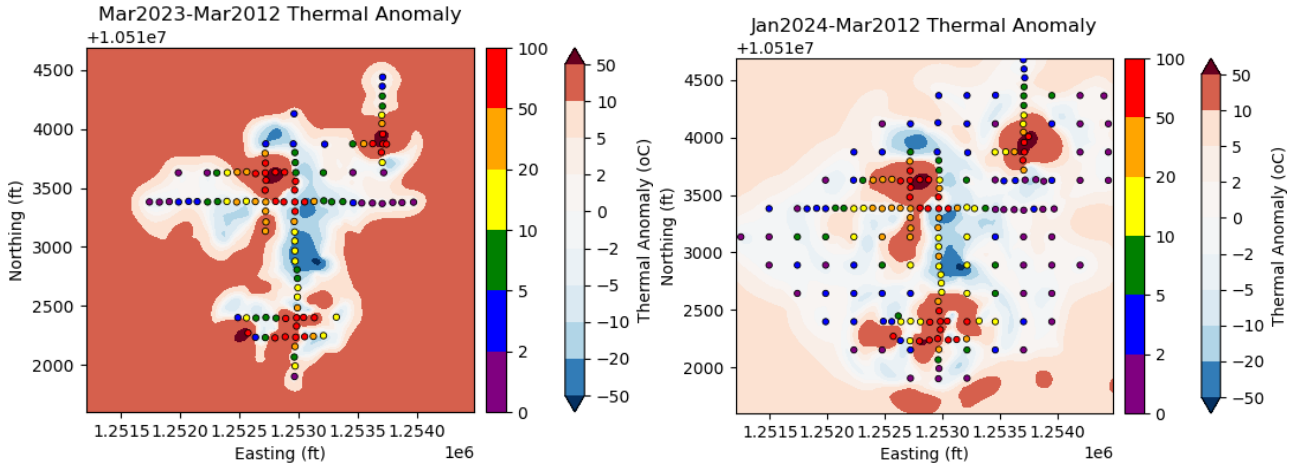

Figure 7: Heat map depicting the difference between the thermal anomaly interpolated across the thermal field between March 2023 and March 2012 (left) and January 2024 and March 2012 (right). Blue values indicate a decrease in temperature, while red values indicate an increase in temperature. The sample locations are represented by circles on the map, and colored based on the most recent temperature results.

Figure 8: Satellite images from Google Earth of the Roosevelt Hot Springs thermal ground from April 2013 and April 2020.

5.4 Background Reading Sensitivity, Variability, and Uncertainty

The lateral extent of the thermal ground is highly sensitive to the selection of the background temperature value. The standard deviation of the background temperatures ranges from 0.1-0.3 in January 2023, up to 0.9-2.3 in October 2023. This shows two things. One, the potential uncertainty in identifying the most appropriate background temperature to correct to. And two, that seasonal differences, such as sun exposure and snow cover, play a significant role in the variability of the background reading. This suggests that generally there is greater certainty in winter measurements, due to less sun exposure and insulating snow cover, than in the fall, when there is greater sunlight, dryer soils, and residual subsurface heat from the summer months.

The variability in background readings also suggests that the background temperature may vary based on environmental conditions such as topography and sun exposure, and thus the "true" background temperature may vary spatially across the field, as well as temporally. For example, the appropriate background temperature on the east side of a ridge may be different that on the west side of the ridge, and they are influenced by different shading patterns throughout the day. Therefore, there could be an increase in error on sunny days.

If the background temperatures are increasing because one or more of the background locations isn't truly background, then this would result in a seemingly colder field, particularly at the very low thermal anomalies that are more sensitive to background conditions. This could explain the apparent cooling occurring across the low temperature parts of the field.

There may also be variability in measurements taken at the same location during the same field trip due to a number of factors such as air temperature, sun exposure (due to changes in cloud cover or shading due to topography and vegetation), and precipitation (rain, snow cover, and snow melt) (Davis and Chapman, 2012). Duplicate readings have been collected at a subset of point locations during the recent survey efforts. Generating a histogram of the variability between duplicate samples can help quantify the uncertainty further.

6. CONCLUSION

The Roosevelt Hot Springs thermal ground area has three main hotspots that reach the local boiling point, resulting in fumaroles, mud pots, and steaming ground. This thermal ground was recently surveyed six times across three seasons over two years to identify changes to the temperature distribution. Seasonal, annual, and decadal trends were considered to identify if the thermal ground region was growing over time, and if so, by how much.

To compare the temperatures across seasons, two correction methods were considered: The thermal anomaly (temperature above background) and normalized temperature (the thermal anomaly over the temperature range from background to boiling point). What was observed is that:

1) The thermal signatures are seasonal, with lower measurable anomalies when the background temperatures are colder.

2) The hot spot areas appear to be expanding, with high temperatures expanding outwards in select directions. This is observed on both the annual and decadal scale.

3) Much of the remaining thermal field, where temperatures are less elevated, appears to be stagnating in temperature, with some regions potentially getting cooler, particularly when viewing the decadal scale differences.

The increase in the hot spot extents could be explained by an increase in the subsurface steam cap, thus increasing the steam flux through the ground surface and increasing the temperature. An alternative explanation could be that the preferential pathways that exist in the hot spots, allowing them to form, are increasing in permeability over time. This could be creating a positive feedback loop, promoting further upflow of subsurface steam in these areas. If part of the thermal field is indeed getting colder, this mechanism could potentially explain this result as well. Further research is necessary to better understand the RHS thermal ground behavior, and understand potential mechanisms for it.

7. FURTHER WORK

This work is ongoing, and a significant amount of further analysis and processing can be performed. To bring the thermal surveys to completion, an additional survey trip is planned for March 2024 to provide a robust dataset from three seasons spaced at 1-yr intervals. This will also provide a March to March 12 year comparison between the 2012 survey by Allis et al., (2019) and present day. Improved geostatistical methods should also be employed, and the kriging parameters further optimized.

The March 2023 soil temperature dataset can be compiled with the drone survey data collected concurrently over the thermal ground by the UGS to support soil temperature interpolation across the unmeasured field. Additional UGS drone surveys have also been conducted between September 2022 and January 2024 to date, and that data may be considered as well. This thermal data should provide a clear picture of how temperature is delineated across the field at the ground surface.

Uncertainty in the background temperatures is a potential concern for interpreting results. An attempt to constrain the potential background temperature values, we anticipate using an approach outlined by Davis and Chapman (2012) to estimate the theoretical background soil temperature. Additional corrections for sun exposure related to topography and time of day/year could also be considered.

Along with temperature, CO_2 flux measurements were collected along the two major transects. This data can be processed in a similar manner to the temperature readings. The two datasets can be considered together as it relates to the evolution of the thermal and steaming ground.

Efforts to model the geothermal reservoir and the influence of geothermal development on the formation of a subsurface steam cap are already underway. Through the combined use of physical measurements from this temperature survey, and simulated processes, the evolution of the post-production Roosevelt Hot Springs system can be better understood.

8. ACKNOWLEDGEMENTS

Funding support for this project provided by the U.S. Department of Energy's (DOE) National Energy Technology Laboratory (NETL) through the Carbon Utilization and Storage Partnership (CUSP) under Award No. DE-FE0031837, which is evaluating CO_2 storage in EGS systems. Additionally, we'd like to acknowledge the assistance of research assistants in gathering the field data, Cassia Tackett, Zella Aspengren, Anna Morrill, Anna Paxton, Noah Paxton, and Kyle Marquardt. Finally, we'd also like to acknowledge those at the Utah Geological Survey (UGS) for their assistance in accessing data and coordinating research efforts: Rick Allis, Christian Hardwick, Kayla Smith, Skadi Kobe, Stefan Kirby, Tyler Knudsen, and Mark Gwynn.

REFERENCES

Allis, R.G., Gwynn, M., Hardwick, C., Kirby, S., Moore, J., and Chapman, D.: Re-evaluation of the pre-development thermal regime of Roosevelt Hot Springs geothermal system, Utah, Proceedings, 40th Workshop on Geothermal Reservoir Engineering, Stanford University, Stanford, CA (2015).

Allis, R.G., and Larsen, G.: Roosevelt Hot Springs Geothermal field, Utah—reservoir response after more than 25 years of power production, Proceedings, 37th Workshop on Geothermal Reservoir Engineering, Stanford University, Stanford, CA (2012).

Allis, R., Gwynn, M., Hardwick, C., Hurlbut, W., Kirby, S.M., and Moore, J.N.: Thermal characteristics of the Roosevelt Hot Springs system, with focus on the FORGE EGS site, Milford, Utah, in Allis, R., and Moore, J.N., editors, Geothermal characteristics of the Roosevelt Hot Springs system and adjacent FORGE EGS site, Milford, Utah: Utah Geological Survey Miscellaneous Publication 169-D, (2019), 22 p.

Davis, M.G., and Chapman, D.S.: A Web-Based Resource for Investigating Environmental Change: The Emigrant Pass Observatory, Journal of Geoscience Education, 60, (2012), 241-248.

Faulder, D.D.: Conceptual geologic model and native state model of the Roosevelt Hot Springs hydrothermal system, Proceedings, 16th Workshop on Geothermal Reservoir Engineering, Stanford University, Stanford, CA (1991), p. 131-142.

Kirby, S.M., Simmons, S., Inkenbrandt, P.C., and Smith, S.: Groundwater hydrogeology and geochemistry of the Utah FORGE site and vicinity, in Allis, R., and Moore, J.N., editors, Geothermal characteristics of the Roosevelt Hot Springs system and adjacent FORGE EGS site, Milford, Utah: Utah Geological Survey Miscellaneous Publication 169-E, (2019), 21 p.

Knudsen, T., Kleber, E., Hiscock, A., and Kirby, S.M.: Quaternary geology of the Utah FORGE site and vicinity, Millard and Beaver Counties, Utah, in Allis, R., and Moore, J.N., editors, Geothermal characteristics of the Roosevelt Hot Springs system and adjacent FORGE EGS site, Milford, Utah: Utah Geological Survey Miscellaneous Publication 169-B, (2019), 21 p.

Nielson, D. L., Evans, S. H., and Sibbett, B. S.: Magmatic, structural, and hydrothermal evolution of the Mineral Mountains intrusive complex, Utah, Geological Society of America Bulletin, 97(6), (1986), 765.

Rahilly, K., Simmons, S., and Fischer, T.P.: Carbon dioxide flux and carbon and helium isotopic composition of soil gases across the FORGE site and Opal Mound fault, Utah, in Allis, R., and Moore, J.N., editors, Geothermal characteristics of the Roosevelt Hot Springs system and adjacent FORGE EGS site, Milford, Utah: Utah Geological Survey Miscellaneous Publication 169-I, (2019), 16 p.